JACS
JOURNAL OF THE AMERICAN CHEMICAL SOCIETY
pubs.acs.org/JACS
Article

Triplet–Triplet Annihilation Upconversion in a Porphyrinic Molecular Container

Hongliang Chen,* Indranil Roy, Michele S. Myong, James S. W. Seale, Kang Cai, Yang Jiao, Wenqi Liu, Bo Song, Long Zhang, Xingang Zhao, Yuanning Feng, Fangjun Liu, Ryan M. Young,* Michael R. Wasielewski,* and J. Fraser Stoddart*

Cite This: J. Am. Chem. Soc. 2023, 145, 10061–10070

Read Online

ACCESS | Metrics & More | Article Recommendations | Supporting Information

ABSTRACT: Triplet–triplet annihilation-based molecular photon upconversion (TTA-UC) is a photophysical phenomenon that can yield high-energy emitting photons from low-energy incident light. TTA-UC is believed to fuse two triplet excitons into a singlet exciton through several consecutive energy-conversion processes. When organic aromatic dyes—i.e., sensitizers and annihilators—are used in TTA-UC, intermolecular distances, as well as relative orientations between the two chromophores, are important in an attempt to attain high upconversion efficiencies. Herein, we demonstrate a host–guest strategy—e.g., a cage-like molecular container incorporating two porphyrinic sensitizers and encapsulating two perylene emitters inside its cavity—to harness photon upconversion. Central to this design is tailoring the cavity size (9.6–10.4 Å) of the molecular container so that it can host two annihilators with a suitable [$\pi\cdots\pi$] distance (3.2–3.5 Å). The formation of a complex with a host:guest ratio of 1:2 between a porphyrinic molecular container and perylene was confirmed by NMR spectroscopy, mass spectrometry, and isothermal titration calorimetry (ITC) as well as by DFT calculations. We have obtained TTA-UC yielding blue emission at 470 nm when the complex is excited with low-energy photons. This proof-of-concept demonstrates that TTA-UC can take place in one supermolecule by bringing together the sensitizers and annihilators. Our investigations open up some new opportunities for addressing several issues associated with supramolecular photon upconversion, such as sample concentrations, molecular aggregation, and penetration depths, which have relevance to biological imaging applications.

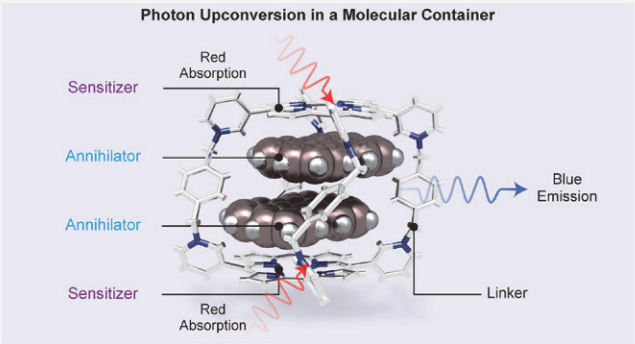

INTRODUCTION

Photon upconversion[1]—a photophysical phenomenon that involves changing low-energy photons into high-energy ones—is a rapidly growing field of research from both fundamental and applied perspectives. Possible applications include photodetectors,[2] solar cells,[3−5] solid-state laser and light-emitting devices,[6−9] in addition to biomedical imaging and theranostics.[10−13] One possible mechanism for this photophysical phenomenon operates through triplet–triplet annihilation-based molecular photon upconversion (TTA-UC).

TTA was first observed in solutions of anthracene more than 60 years ago.[14−16] Since then, the concept of using two functional components—i.e., a sensitizer (Sn) and an annihilator (An)—to convert light energies has been adopted[1,16−18] widely within the scientific community. The energy-transfer steps of TTA-UC often proceed as follows: first, a sensitizer in its ground state (^{1}Sn) is excited (Figure 1a) to a singlet excited state (^{1}Sn*) by absorbing low-energy incident photons before undergoing intersystem crossing (ISC), leading to a triplet exciton (^{3}Sn*). Second, an annihilator (^{1}An)—whose triplet state (^{3}An*) energy is lower than the triplet exciton (^{3}Sn*) of the sensitizer—is excited to ^{3}An* as a result of efficient triplet energy transfer (TET) from the sensitizer to the annihilator. Finally, TTA occurs between two annihilators (^{3}An*), resulting in the generation of one singlet exciton (^{1}An*) and the emission of high-energy photons.

Porphyrin and perylene derivatives are among the most promising and effective sensitizer/annihilator pairs of dyes used in TTA-UC applications.[19,20] Porphyrin[21,22] is a light-absorbing photosensitizer with several absorption peaks located in the red and even near-infrared regions. Perylene, acting as an annihilator, has demonstrated[23−26] high

Received: December 29, 2022
Published: April 25, 2023

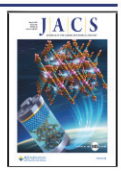

https://doi.org/10.1021/jacs.2c13846
J. Am. Chem. Soc. 2023, 145, 10061–10070

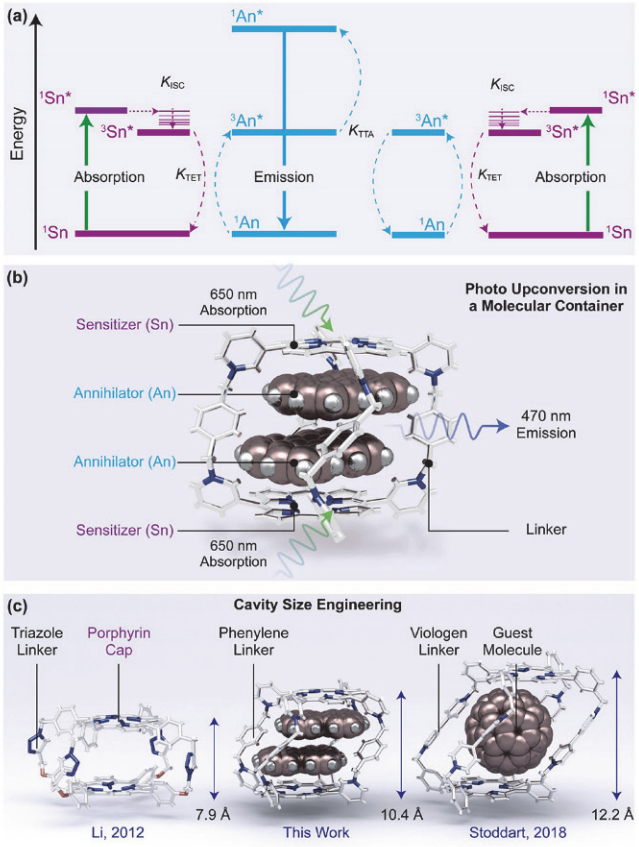

Figure 1. Design of an upconverted porphyrinic molecular container. (a) Schematic energy-level diagram of TTA upconversion. (b) Schematic illustration showing that the sensitizers and annihilators are bound in a molecular container courtesy of host–guest chemistry. (c) Supramolecular engineering leading to the preparation of a porphyrinic molecular container with the plane-to-plane distance of 10.4 Å between the floor and roof provided by two porphyrins.

fluorescence quantum yields with robust photostability. The similar triplet energies of porphyrins and perylene make them viable candidates for TTA-UC. In addition to these properties, intermolecular distances between a sensitizer and an annihilator, as well as their superstructures and relative orientations, are also important in attempts to obtain[27−30] high upconversion efficiencies. We envision that (Figure 1b) if upconversion can be achieved in a molecular container[31−33]—wherein sensitizers and annihilators are bound together in a host–guest complex[34−38]—it could offer the opportunity to overcome[39−41] the challenges associated with intermolecular distances and relative orientations of sensitizers and annihilators. In this context, we designed (Figure 1b) a three-dimensional porphyrinic molecular container with two porphyrin sensitizers serving as the roof and floor, thus enabling the encapsulation of annihilators in the form of two large perylene molecules.

The use of porphyrins extends[42−50] the dimensions of the molecular container. The challenge, however, lies in the engineering of the cavity size that allows the molecular container to host two annihilators. Considering that the averaging [$\pi\cdots\pi$] stacking distance[51] is 3.3 to 3.5 Å, the distance separating the roof and floor should be located in the range of 9.9 to 10.5 Å. In 2012, Li[52] prepared a zinc porphyrin cage using four triazole units as linkers. A single-crystal X-ray structure revealed that (Figure 1c, left) the distance between the two Zn atoms was 7.9 Å, resulting in a cavity that is too small to host[53,54] two π-conjugated guest molecules. In 2018, we[42] described a three-dimensional porphyrinic molecular container, **TPPCage**$^{8+}$, which is composed of two porphyrins linked by four viologen units in a rhomboid prismatic manner. Although the enlarged cavity size (12.2 Å) of **TPPCage**$^{8+}$ allows (Figure 1c, right) the encapsulation[55−65] of large fullerene guests, it fails to confine[66−68] two π-conjugated guests because of their weak binding affinities. Here, we report the synthesis (Scheme 1) of a porphyrinic molecular container (Figure 1c, middle)—namely, **PorCage**$^{8+}$, in which 5,10,15,20-tetra(pyridin-3-yl)porphyrins serve as the roof and floor separated by four *p*-xylylene linkers. The use of four pyridine units with their meta-positions connected to the 5,10,15,20-positions on the porphyrin is the key design element of this cage. The partial rotation of four pyridine units allows the stretching and compressing of the nanocage, leading to the fine tuning of the cavity size to ∼10.4 Å and successful encapsulation of two perylene guest molecules. When the porphyrins in the complex are excited with low-energy light, the upconverted fluorescence at 470 nm originates from the perylene guests. This research offers a new strategy in molecular engineering for the rational design of molecular containers along with prospects for controlling the host–guest chemistry as well as the photophysical properties of the host–guest complex.

■ EXPERIMENTAL SECTION

Synthesis of PorCage^{8+}. **PorCage**·8PF$_6$ was prepared (Scheme 1) by a couple of successive S_N2 reactions from commercially available materials—i.e., 5,10,15,20-tetra(pyridin-3-yl)porphyrin (**TPP**) and 1,4-bis(bromomethyl)benzene. The intermediate, **TPP**·4PF$_6$, was obtained from the substitution of the four pyridines with an excess of 1,4-bis(bromomethyl)benzene in DMF at 100 °C. Cage formation was performed in MeCN at 110 °C by employing **TPP** and **TPP**·4PF$_6$ as starting materials in the presence of tetra-*n*-butylammonium iodide (TBAI) as a catalyst. This reaction proceeds very slowly and takes between 14 to 30 days to go to completion on account of the low solubility of **TPP** in MeCN. The synthesis was

Scheme 1. Synthesis of PorCage·8PF$_6$

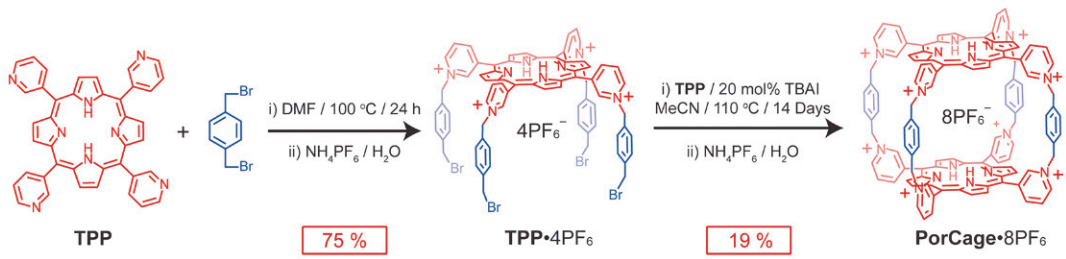

https://doi.org/10.1021/jacs.2c13846
J. Am. Chem. Soc. 2023, 145, 10061−10070

completed by collecting the precipitate directly from the reaction solution—bypassing the use of column chromatography—followed by counterion exchange (NH_4PF_6/H_2O). The isolated yield of **PorCage**·$8PF_6$ was ~19%.

Characterization of PorCage^{8+}. The structure of **PorCage^{8+}** in solution was confirmed by one-dimensional (1D) ^{1}H (Figure S1) and ^{13}C (Figure S2) NMR spectroscopy. Each peak in the ^{1}H NMR spectra was assigned unambiguously based on a variety of two-dimensional (2D) NMR spectroscopic investigations, namely, ^{1}H−^{1}H COSY (Figure S3), NOESY (Figure S4), ^{1}H−^{13}C HSQC (Figure S5), and HMBC (Figure S6). ESI-MS spectrometry confirmed (Figure S13) the formation of **PorCage**·$8PF_6$ by indicating the presence of $[M-2PF_6]^{2+}$ and $[M-3PF_6]^{3+}$ ions with m/z values of 1261.25 and 792.51, respectively.

Purple-colored single crystals of **PorCage**·$8PF_6$ were grown by slow diffusion over the course of 4 days of i-Pr_2O into **PorCage**·$8PF_6$ dissolved in MeCN. The solid-state (super)structure of **PorCage**·$8PF_6$ (Figure S14) reveals that the molecular container crystallizes in the *Pmma* space group. It consists of two parallel tetra(pyridin-3-yl)porphyrins linked by four *p*-xylylene units. **PorCage^{8+}** adopts (Figure 4a−c and Figure S14) a cage-like geometry, with average dimensions of 10.4 × 10.3 × 11.4 Å. The centroid-to-centroid distance (10.4 Å) between the two porphyrins is smaller than the corresponding distance[42] (12.2 Å) in **TPPCage^{8+}** (Figure 1c, right). Considering an average $[\pi\cdots\pi]$ interaction distance of 3.4 Å, we envision that the "open window"—the distance between two porphyrins—in **PorCage^{8+}** will accommodate two π-conjugated planar guests in its cavity (3.4 Å × 3 = 10.2 Å). The solid-state superstructure of **PorCage^{8+}** reveals (Figure S14) that it crystallizes in a layer-by-layer manner—utilizing $[\pi\cdots\pi]$ interactions between porphyrins in adjacent cages—with plane-to-plane distances of ~3.3 Å.

■ RESULTS AND DISCUSSION

Host−Guest Complex Formation. The perfectly crafted cavity inside the molecular container, in addition to the affinity of the porphyrins for **Perylene**, courtesy of $[\pi\cdots\pi]$ interactions, ensures that the **PorCage^{8+}** acts as a good molecular container for the accommodation of two **Perylenes**. The formation of the 1:2 complex was confirmed by traditional means, i.e., ^{1}H and ^{13}C NMR spectroscopy and mass spectrometry, as well as by isothermal titration calorimetry (ITC). Upon addition of excess (5 equimolar) **Perylene** into a MeCN solution of **PorCage^{8+}**, the ^{1}H NMR spectra reveal (Figure 2b−d) significant changes in chemical shifts for both **Perylene** and **PorCage^{8+}** protons in keeping with complex formation between **Perylene** and **PorCage^{8+}**. Peaks in the ^{1}H NMR spectra of the host, the guest, and the 1:2 complex were assigned based on 2D NOESY (Figure 3b), COSY (Figure S7), ROESY (Figure S8), HSQC (Figure S9), and HMBC (Figure S10) spectra. As indicated by the red dashed lines in Figure 2, the chemical shifts of H-e and H-d on the pyridinium units and H-p on the porphyrins show (Figure 2c,d) upfield shifts ($\Delta\delta$ = −0.80, −0.27, and −0.61 ppm for H-e, H-d, and H-p, respectively), while protons H-c and H-f on the pyridinium units and H-a and H-b on the *p*-xylylene linkers display downfield shifts ($\Delta\delta$ = 0.07, 0.19, 0.69, and 0.38 ppm for H-c, H-f, H-a, and H-b, respectively). These changes in chemical shifts indicate that the chemical environment inside **PorCage^{8+}** is altered on account of the inclusion of the **Perylene** guest molecules inside the cavity, forming a 1:2 complex. The aromatic protons on **Perylene** that resonate (Figure 2a) at δ 8.30, 7.76, and 7.53 ppm for H-A, H-C, and H-B, respectively, are separated (Figure 2d) into two sets of signals—i.e., (i) those exhibiting a large upfield shifts with δ = 5.57 for H-A′ and δ = 3.82 for the overlapping resonances for H-C′ and H-B′ and (ii) those exhibiting small upfield shifts with δ = 8.23, 7.72, and 7.50 ppm for H-A″, H-C″, and H-B″, respectively. The first set of peaks is assigned to the protons (H-A′, H-B′, and H-C′) of the **Perylenes** that are encapsulated inside the cavity of **PorCage^{8+}**. The second set is assigned to protons (H-A″, H-B″, and H-C″) in **Perylenes** that are located outside the cavity of **PorCage^{8+}**.

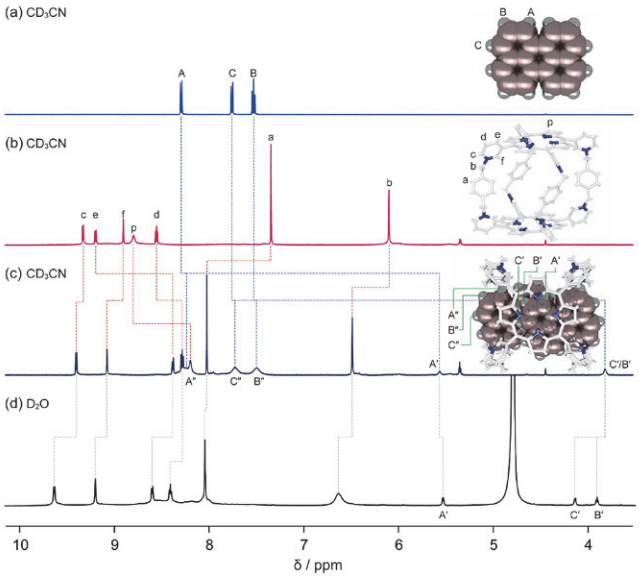

Figure 2. ^{1}H NMR spectroscopy of the molecular container. (a−c) Stacked ^{1}H NMR spectra (500 MHz, CD_3CN, 298 K) of **Perylene** (a), **PorCage**·$8PF_6$ (b), and **PorCage**·$8PF_6$ ⊃ **2Perylene** (c) with proton assignments. (d) ^{1}H NMR spectrum (600 MHz, D_2O, 298 K) of **PorCage**·$8PF_6$ ⊃ **2Perylene** with proton assignments.

An ^{1}H NMR spectrum in D_2O demonstrated (Figure 2d) a similar result except for the broadening of H-b and the separation of the overlapping resonances for H-C′ and H-B′. These phenomena indicate that the complexation of **PorCage^{8+}** ⊃ **2Perylene** in D_2O is less dynamic than that in MeCN. An ^{1}H NMR titration demonstrated (Figure S11) that the complex between the first **Perylene** and **PorCage^{8+}** undergoes slow exchange on the ^{1}H NMR time scale. A variable-temperature ^{1}H NMR experiment was performed (Figure S12) on a 1:2 molar mixture of **PorCage**·$8PF_6$ and **Perylene**. Upon lowering the temperature from 20 to −30 °C, resonances for H-B″ and H-C″ gradually appear, signaling that the second **Perylene** is experiencing fast exchange. A 2D ^{1}H−^{1}H NOESY spectrum (Figure 3b) shows through-space interactions between C″−A′, B″−C′, and A″−B′, indicating that two **Perylenes** are bound as a pair of molecules inside the cavity of **PorCage^{8+}**.

ESI-MS is another powerful technique that can provide evidence for complex formation. In an MeCN solution containing a 1:2 equimolar mixture of **PorCage^{8+}** and **Perylene**, several new peaks appear (Figure 3c) in the ESI-MS. The emergence of m/z peaks at 684.20 and 960.59 confirms (Figure 3c, red) the formation of the 1:2 complex **PorCage^{8+}** ⊃ **2Perylene**. Signals for the 1:1 **PorCage^{8+}** ⊃ **Perylene** complex are also obtained (Figure 3c, green), with m/z values in its mass spectrum at 621.17 and 876.54, which can be attributed to the dynamic nature of the host−guest complex in MeCN. The isotopic patterns (Figure 3c, inset, blue) with four and three positive charges at m/z = 684.20 for $[$**PorCage**·$4PF_6]^{4+}$ ⊃ **2Perylene** and at m/z = 960.59 for

https://doi.org/10.1021/jacs.2c13846
J. Am. Chem. Soc. 2023, 145, 10061−10070

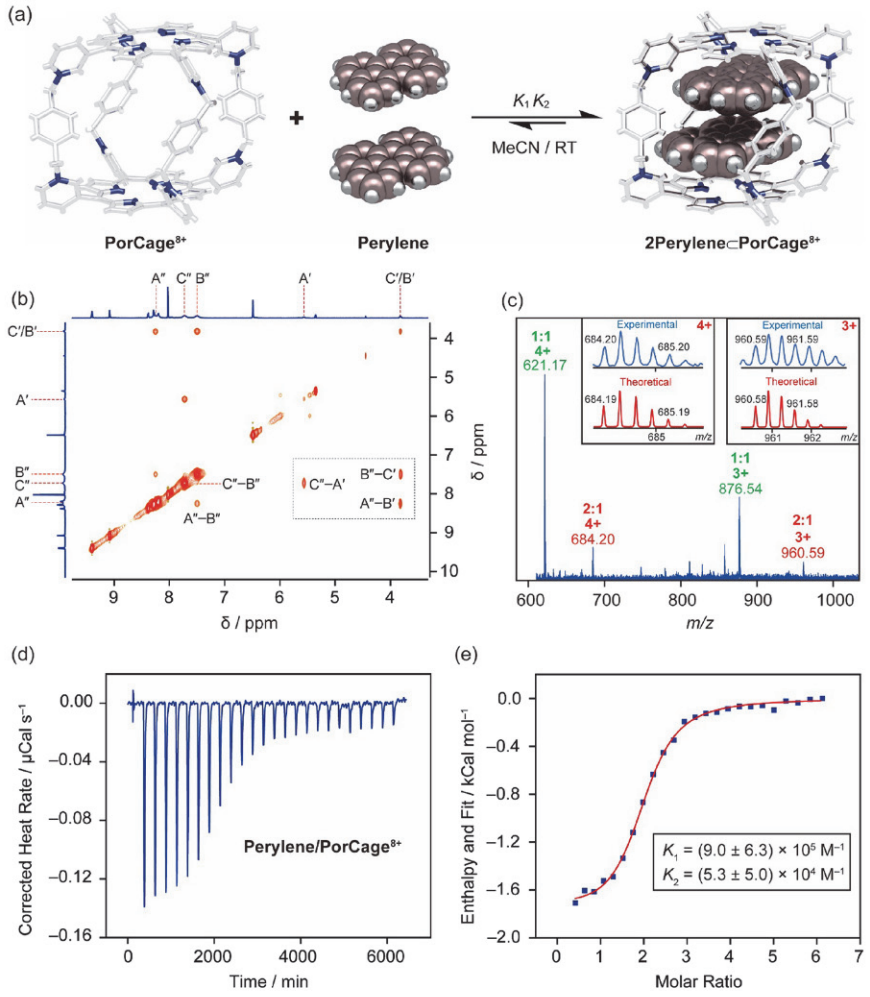

Figure 3. Formation of host–guest complexes. (a) Schematic illustration showing the inclusion of two **Perylene** guest molecules in **PorCage**$^{8+}$. (b) ^{1}H–^{1}H NOESY (500 MHz, CD_3CN, 298 K) characterization of **PorCage**$^{8+}$ ⊃ **2Perylene**. Protons are labeled on relevant structural formulas in Figure 2c. (c) Electrospray ionization mass spectra (ESI-MS) of **PorCage**$^{8+}$ ⊃ **2Perylene**. (d) Isothermal titration calorimetry (ITC) results from adding **Perylene** (500 μM, in syringe) to **PorCage**$^{8+}$ (25 μM, in cell) at 298 K in MeCN. (e) Nonlinear fitting of enthalpy using a 1:2 host:guest binding model.

[**PorCage**·5PF_6 ⊃ **2Perylene**]$^{3+}$ are well matched with the theoretical values (Figure 3c, inset, red), a phenomenon that confirms the formation of a complex with a 1:2 molar ratio.

In order to gain more information about the 1:2 complex formed between **PorCage**·8PF_6 and **Perylene**, the binding constants were determined (Figure 3d,e and Figure S16) by ITC in MeCN. The titration curve matches (Figure 3e) that of a 1:2 binding model with averaged binding constants of K_1 = (9.0 ± 6.3) × 10^5 M^{-1} and K_2 = (5.3 ± 5.0) × 10^4 M^{-1}. In-depth analyses of the ITC results reveal that the recognition between **PorCage**$^{8+}$ and **Perylene** is the result of (Table S1) an exothermal process where the binding enthalpies are determined to be ΔH_1 = −1.70 kcal mol^{-1} and ΔH_2 = −0.92 kcal mol^{-1}, respectively. UV–vis titration experiments were performed (Figure S18a) subsequently by recording the absorbance changes at 588 nm. The plotted data also match a 1:2 binding model, giving (Figure S18b) binding constants of K_1 = 1.8 × 10^6 M^{-1} and K_2 = 6.1 × 10^3 M^{-1}. The mechanism and driving force behind one and two guest molecules being included into the cavity of **PorCage**$^{8+}$, however, is complicated and beyond the scope of the current research. Based on the ^{1}H NMR spectroscopic measurements, ESI-MS experiments, ITC, and UV–vis titration, we conclude that a 1:2 complex can be assembled by mixing the **PorCage**·8PF_6 with 2 molar equivalents of **Perylene** in MeCN.

DFT Calculations. Density functional theory (DFT) calculations were performed (SI) on a **PorCage**$^{8+}$ ⊃ **2Perylene** complex in order to gain a better understanding of the relationship between its superstructure and photophysical properties. The **PorCage**$^{8+}$ ⊃ **2Perylene** complex adopts (Figure 4e–g) a cage-like geometry that is similar to that of the empty **PorCage**$^{8+}$ in its solid-state structure. The average size of the complex (Figure S24), however, changes ever so slightly on account of the encapsulation of guest molecules. For example, two porphyrins are compelled to be compressed—with the centroid-to-centroid distance being reduced (Figure 4d) from 10.4 to 9.6 Å. The *p*-xylylene pillars are forced to bend, with the distances (Figure 4f) between any two contiguous *p*-xylylene units being increased to 10.8 Å. Two **Perylene** guest molecules adopt (Figure 4g–i) a parallel but slightly displaced π-stacking geometry with an average [$\pi\cdots\pi$] distance of ∼3.3 Å. Independent gradient model (IGM) analysis demonstrates (Figure 4j and Figure S25) that the two **Perylenes** are enveloped by attractive van der Waals contacts

https://doi.org/10.1021/jacs.2c13846
J. Am. Chem. Soc. 2023, 145, 10061–10070

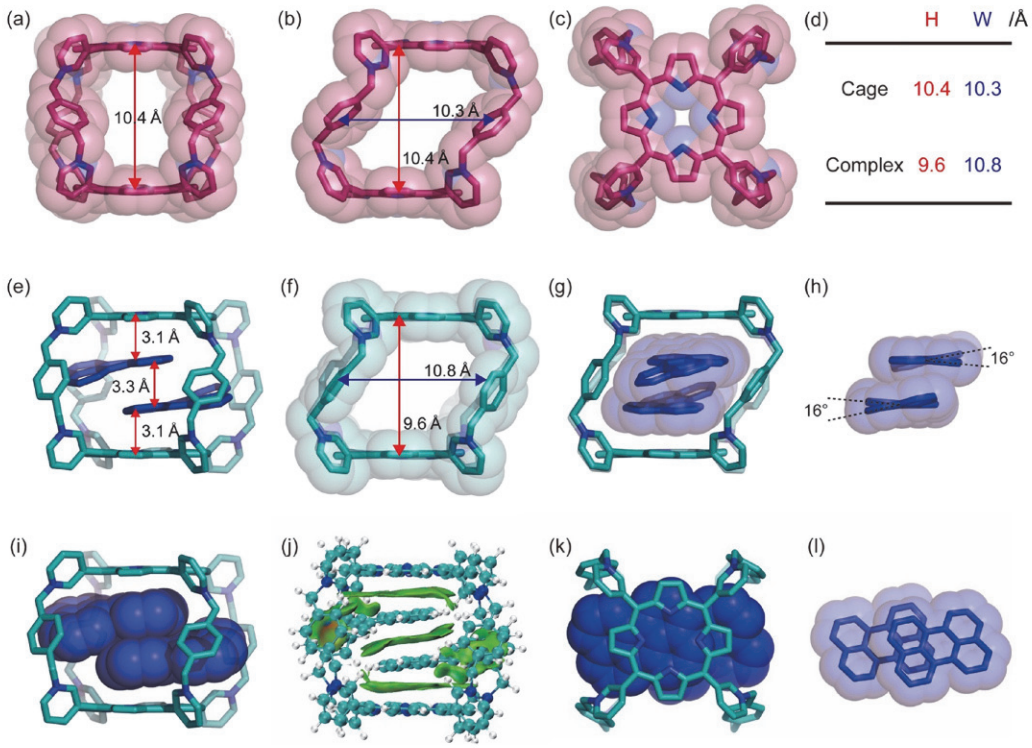

Figure 4. Solid-state (super)structures of the cage and complex. (a–c) Space-filling representation of the solid-state structure of the **PorCage**$^{8+}$ obtained by X-ray crystallography showing the dimensions of the cage with front (a), side-on (b), and top-down (c) views. (e) Capped-stick representation showing the optimized superstructure of **PorCage**$^{8+}$ ⊃ **2Perylene** obtained from DFT calculations. (f) Space-filling representation showing an individual **PorCage**$^{8+}$ in the complex with compressed dimensions. Side-on views ((g) and (h), respectively) of the superstructures of **PorCage**$^{8+}$ ⊃ **2Perylene** and individual **Perylene** guests. Front view (i) of the superstructure showing a parallel displaced co-conformation for the **Perylene** dimer. Intermolecular [$\pi\cdots\pi$] binding isosurface (j) of **PorCage**$^{8+}$ ⊃ **2Perylene**. Top-down views ((k) and (l), respectively) showing the superstructures of the complex and individual **Perylene** guests.

with the roof and floor in **PorCage**$^{8+}$ as well as between the two **Perylene** guests. It transpires that the parallel but displaced π-stacking geometry of the two **Perylenes** (Figure 4k,l) leads to portions of the two **Perylenes** being located outside the molecular container, resulting in reduced shielding effects for H-A″, H-B″, and H-C″ in the ^{1}H NMR spectrum (Figure 2c).

Steady-State Photophysical Studies. The steady-state absorption spectrum (Figure S17) of **PorCage**$^{8+}$ in MeCN shows a strong porphyrin Soret band centered around 425 nm and four characteristic porphyrin Q bands with absorption maxima at 518, 550, 585, and 640 nm. The absorption spectrum (Figure S17) of **Perylene** in MeCN exhibits three characteristic peaks centered around 390, 415, and 440 nm. A 1:2 mixture of **PorCage**$^{8+}$ and **Perylene** in MeCN, on the other hand, exhibits broadening of the porphyrin Soret and Q bands in keeping with the complexation between **PorCage**$^{8+}$ and **Perylenes**. The band at 430 nm has contributions from both the **PorCage**$^{8+}$ and the **Perylenes**. As the complexation in MeCN is dynamic, the charge transfer (CT) band is not prominent, an observation that is consistent with an earlier study[35] on supramolecular photon upconversion.

The steady-state absorption (Figure 5a) of **PorCage**·8Cl ⊃ **2Perylene** in H_2O (20 μM) includes the spectral features of **PorCage**$^{8+}$—i.e., (i) the porphyrin Soret band with a maximum absorption at around 420 nm, and (ii) the porphyrin Q bands centered around 520, 555, 590, and 650 nm. As the host–guest complexation is no longer dynamic in water, a weak CT band is observed between 650 and 850 nm, an observation that corroborates[34] the results obtained from DFT calculations where the HOMO is located on the **Perylene** and LUMO on the **PorCage**$^{8+}$.

When the aqueous solution of **PorCage**·8Cl and **Perylene** is excited (Figure 5b) with low-energy light with wavelengths of 650 and 700 nm, upconverted fluorescence (UCF) signals originating from **Perylenes** can be detected between 425 and 525 nm with an emission maximum at 470 nm and anti-Stokes shifts of 0.73 and 0.87 eV, respectively. The dependence of UCF intensity as a function of the incident light power density at 650 nm excitation was also measured and plotted in Figure 5c. The UCF intensity increases with increasing excitation power density. Quantitatively, the UCF intensity displays (Figure 5c, inset) a double-logarithmic relationship with the excitation power density. The plot demonstrates a quadratic-to-linear transition with slopes of ~2 and ~1, revealing that a triplet-fusion upconversion process occurs in the complex. The threshold of excitation power density, with a value estimated to be 11.5 mW cm^{-2}, is deduced (Figure 5c, inset) from the intersection of the two slopes. The low ΔE_{ST} = 0.76 eV obtained (Figure S31) from the DFT experiment also supports the involvement of efficient intersystem crossing ($S_1 \rightarrow T_1$) in **PorCage**·8Cl. Importantly, the perylene-based emission from **PorCage**·8Cl ⊃ **2Perylene** shows a red-shifted 0–0 band compared to the free monomer, which is likely a result of the strong [$\pi\cdots\pi$] interactions between the stacked **perylenes** within the cavity, possibly resulting[69] in excimer-like emission. The ability to contain π-stacked dimers within the cavity allows for accessing longer-lived emissive states from such excimers

https://doi.org/10.1021/jacs.2c13846
J. Am. Chem. Soc. 2023, 145, 10061–10070

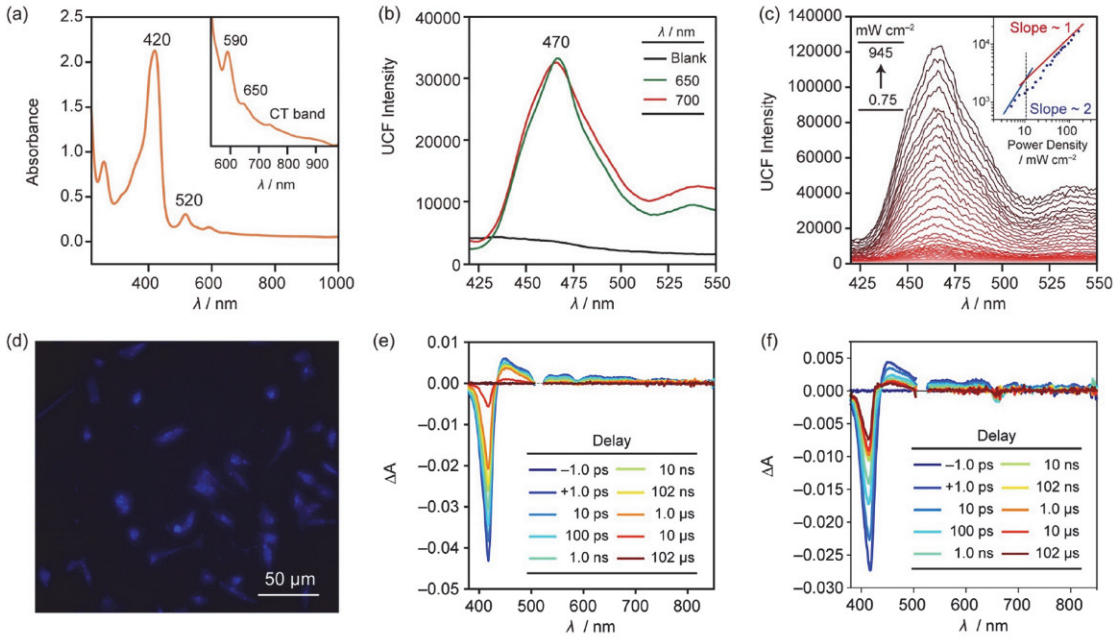

Figure 5. Absorption, emission, and transient absorption of the complex. (a) UV−vis absorption spectrum of **PorCage**·8Cl ⊃ **2Perylene** in H_2O. Inset shows the CT band of the complex. (b) Fluorescent emission of **PorCage**·8Cl ⊃ **2Perylene** at 470 nm in de-aerated H_2O with different excitation wavelengths. (c) Dependence of UCF intensity at 470 nm of **PorCage**·8Cl ⊃ **2Perylene** in H_2O with respect to the incident light intensity. Inset shows a plot of excitation power density versus UCF intensity. (d) In vitro imaging of **PorCage**·8Cl ⊃ **2Perylene** in DU145 cells using confocal laser scanning microscopy following excitation at 600 nm. (e) Transient absorption spectra of **PorCage**·8Cl and (f) **PorCage**·8Cl ⊃ **2Perylene** in H_2O at various time delays after excitation at 515 nm.

that would not generally be available in different TTA-UC platforms.[35]

The relative upconversion fluorescence quantum yields of **PorCage**·8Cl ⊃ **2Perylene** in H_2O and **PorCage**·8PF_6 ⊃ **2Perylene** in MeCN with the standard of CdSe/CdS core shell quantum dot in toluene were calculated to be 0.3 and 0.19%, respectively. In view of the good hydrophilicity of the **PorCage**·8Cl ⊃ **2Perylene** complex with UCF characteristics, biomedical applications for cancer-cell imaging have been investigated[70] (Figure 5d). The in vitro investigations in DU145 cells by confocal laser scanning microscopy confirm the uptake of the **PorCage**·8Cl ⊃ **2Perylene** complex into cancer cells and the intracellular emissions of blue UCF signals. The UCF signals are distributed evenly in the cytoplasm of the DU145 cells, demonstrating that the **PorCage**·8Cl ⊃ **2Perylene** complex can probe cancer cells effectively.

Excited State Dynamics of Porphyrin Cage and Complex. Transient absorption (TA) spectroscopy was used to explore the suitability of **PorCage**·8Cl for TTA-UC and the upconversion mechanism in **PorCage**·8Cl ⊃ **2Perylene** in H_2O and **PorCage**·8Cl ⊃ **2Perylene** in MeCN and to compare to the dynamics of the free **PorCage**$^{8+}$. A necessary requirement for an efficient TTA-UC sensitizer is a long triplet lifetime in solution. Selective excitation of the porphyrin Q band at λ_{ex} = 515 nm in each case shows (Figures S20−23) the formation of the porphyrin first singlet excited-state S_1 with a broad excited-state absorption (ESA) band peaking near 450 nm, along with a prominent negative ground-state bleach of the Soret band at 418 nm and depressions in the ESA on account of bleaching of the Q bands near 518, 555, 590, and 650 nm.

In H_2O, the singlet excited state of the unbound ^{1}***PorCage**·8Cl (Figure 5e and Figure S20) undergoes structural relaxation processes in 4, 40, and 650 ps on account of the semi-rigid nature of the cage, where the singlet ESA features are fully maintained but some population is lost because of fluorescence and internal conversion. Relaxation on S_1 is followed by ISC with a time constant of 10.3 ± 0.2 ns; this process manifests as a redshift in the ESA peak maximum. The triplet state decays with a lifetime of ∼660 μs in de-aerated water on account of collisional quenching with other porphyrin triplets in solution. The intrinsic triplet lifetime of a free base tetraphenyl poprphyrin (H_2TPP) is determined[71] to be ∼6 ms, so the observed incomplete decay on the ∼340 μs time window of our experiment in the absence of oxygen must result from diffusional quenching.

The singlet excited state of ^{1}***PorCage**·8Cl ⊃ **2Perylene** (Figure 5f and Figure S21) undergoes similar relaxation (3.5, 52.6, and 740 ps) prior to intersystem crossing in 10.0 ± 0.1 ns. The subtle changes in relaxation are likely originate from the increased rigidity of the complex compared to the free cage, while the intersystem crossing time is unchanged within the error of the experiment. The triplet state similarly has a lifetime of ∼500 μs.

Similar dynamics of both the free cage and the complex are observed in MeCN (Figures S22 and S23), though the dynamic nature of the binding leads to more complicated kinetics on account of the presence of multiple, parallel excited-state populations from the distribution of free and bound cages. Using the same kinetic model, we observe that both the free cage and complex undergo similar relaxation of the singlet state prior to intersystem crossing with comparable ∼9 ns lifetimes. The largest difference is the significantly shorter triplet lifetime (4 and 6 μs, respectively) because of the lower viscosity of MeCN leading to faster diffusion of the triplet states. These lifetimes are still suitable for TTA-UC, as discussed below.

https://doi.org/10.1021/jacs.2c13846
J. Am. Chem. Soc. 2023, 145, 10061−10070

Importantly, no ^{3}*Perylene is observed in the TA experiment, though its presence is required, albeit transiently, to explain the perylene emission in the steady-state data. The reason for this observation lies with the precise energetic ordering of the sensitizer and annihilator triplet levels. The experimental triplet energy of the perylene annihilator was determined[72] to be 1.53 eV (though it is possible that the triplet energy is lowered upon π-stacking in the cavity), while that of the unmetallated porphyrin derivative used here as the annihilator is unreported. The triplet energy of H_2TPP has been measured[71] to be 1.45 eV and may be taken as a surrogate triplet energy for the porphyrins used in the cage structure. Thus, even though the sensitizer−annihilator triplet energy gap ΔE_{TT} is small, TTA-UC is still endoergic by −80 meV and is therefore thermally activated. At room temperature, triplet−triplet energy transfer would only be $(-\Delta E_{TT}/k_BT)$ = ∼4% efficient, an observation which is consistent with the small but non-negligible TTA-UC signal observed in the steady-state experiments. In the transient absorption experiments, however, the majority of the porphyrin triplet population does not undergo energy transfer and the fraction that does produces a perylene $T_n \leftarrow T_1$ absorption that overlaps strongly with that of the porphyrin, near 460 nm, and as such would be difficult to observe.[73,74] The change in triplet lifetime upon complexation with two perylene units may be indicative of triplet energy-transfer in some of the population. Since the triplet decay is dominated by diffusional quenching between excited porphyrins in solution, however, the difference in rate constant may only be reflecting small changes in concentration.

Despite the low probability of triplet−triplet energy transfer, the nature of the illumination in the steady-state emission measurements makes the observation of TTA-UC viable. Continuous excitation of the sensitizer will lead to a constant turnover of triplet population such that even a relatively inefficient triplet energy transfer process can lead to appreciable TTA-UC signals. This is also true for intramolecular TTA-UC, which requires each complex to absorb two incident photons to produce two sensitizer-excited states. Under the pulsed excitation conditions of the TA experiment, the probability of double excitation[75] is only around 2%, meaning that the TA data are again dominated by populations of singly excited complexes. Continuous excitation, however, makes the probability of multiple excitations on one assembly within the triplet excited-state lifetime substantial over the collection time, a situation which is consistent with the observed TTA-UC yields. Hence, even the few-microsecond lifetimes in MeCN are still sufficient to accumulate triplet excitations on a single assembly, while the <1-ms lifetimes in H_2O provide even more opportunity for TTA-UC. A particular pump and probe technique may be utilized[76] in order to observe the annihilator triplet lifetime directly in the confined TTA-UC system in future studies.

TTA-UC efficiency may be substantially improved by metalating the porphyrins in the cage with Zn. The measured triplet energy of ZnTPP, for example, was found[77] to be 1.55 eV, which is 100 meV higher than that of the freebase porphyrin and higher than the triplet state of the perylene annihilator, thus making triplet−triplet energy transfer much more probable. Triplet lifetimes can be further extended in more viscous solvents, frozen solutions, or even the solid state where diffusional quenching is hindered or prevented. The ability of this system to undergo TTA-UC without diffusion is unique to supramolecular assemblies such as those described in this paper.

CONCLUSIONS

In this research, we have investigated the triplet−triplet annihilation-based molecular photon upconversion properties of a complex in which two guest annihilators (perylenes) are encapsulated inside a porphyrinic molecular container with two porphyrins as the sensitizers. When the Q bands of the porphyrins are excited with low-energy light, the upconverted fluorescence of the perylenes at 470 nm can be detected. Central to this research is the integration of two sensitizers and two annihilators in a complex with a 1:2 host−guest ratio. As a result, the key function of the molecular container is to tune its cavity size in order to make the container suitable to host two π-conjugated guest annihilators with a $[\pi\cdots\pi]$ distance in the range of 3.2−3.5 Å. These results demonstrate the importance of molecular engineering in controlling the geometry of host−guest complexes as well as their photophysical properties. Supramolecular photon upconversion strategies will aid in the development of new materials and chemistries as they relate to electrical, photophysical, and biomedical applications.

ASSOCIATED CONTENT

Supporting Information

The Supporting Information is available free of charge at https://pubs.acs.org/doi/10.1021/jacs.2c13846.

Further experimental details, computational methods, and DFT calculation results (PDF)

Accession Codes

CCDC 2213858 contains the supplementary crystallographic data for this paper. These data can be obtained free of charge via www.ccdc.cam.ac.uk/data_request/cif, or by emailing data_request@ccdc.cam.ac.uk, or by contacting The Cambridge Crystallographic Data Centre, 12 Union Road, Cambridge CB2 1EZ, UK; fax: +44 1223 336033.

AUTHOR INFORMATION

Corresponding Authors

Hongliang Chen − *Department of Chemistry, Stoddart Institute of Molecular Science, Zhejiang University, Hangzhou 310027, China; Department of Chemistry, Northwestern University, Evanston, Illinois 60208, United States; ZJU-Hangzhou Global Scientific and Technological Innovation Center, Hangzhou 311215, China;* orcid.org/0000-0002-4442-7984; Email: hongliang.chen@zju.edu.cn

Ryan M. Young − *Department of Chemistry, Northwestern University, Evanston, Illinois 60208, United States;* orcid.org/0000-0002-5108-0261; Email: ryan.young@northwestern.edu

Michael R. Wasielewski − *Department of Chemistry, Northwestern University, Evanston, Illinois 60208, United States;* orcid.org/0000-0003-2920-5440; Email: m-wasielewski@northwestern.edu

J. Fraser Stoddart − *Department of Chemistry, Stoddart Institute of Molecular Science, Zhejiang University, Hangzhou 310027, China; Department of Chemistry, Northwestern University, Evanston, Illinois 60208, United States; ZJU-Hangzhou Global Scientific and Technological Innovation Center, Hangzhou 311215, China; School of Chemistry, University of New South Wales, Sydney, NSW 2052,*

Australia; orcid.org/0000-0003-3161-3697; Email: stoddart@northwestern.edu

Authors

Indranil Roy – *Department of Chemistry, Northwestern University, Evanston, Illinois 60208, United States;* orcid.org/0000-0003-3288-2207

Michele S. Myong – *Department of Chemistry, Northwestern University, Evanston, Illinois 60208, United States;* orcid.org/0000-0003-3634-8933

James S. W. Seale – *Department of Chemistry, Northwestern University, Evanston, Illinois 60208, United States;* orcid.org/0000-0001-8086-6020

Kang Cai – *College of Chemistry, Nankai University, Tianjin 300072, China;* orcid.org/0000-0002-8883-0142

Yang Jiao – *Department of Chemistry, Northwestern University, Evanston, Illinois 60208, United States*

Wenqi Liu – *Department of Chemistry, Northwestern University, Evanston, Illinois 60208, United States;* orcid.org/0000-0001-6408-0204

Bo Song – *Department of Chemistry, Northwestern University, Evanston, Illinois 60208, United States;* orcid.org/0000-0002-4337-848X

Long Zhang – *Department of Chemistry, Northwestern University, Evanston, Illinois 60208, United States;* orcid.org/0000-0002-4631-158X

Xingang Zhao – *Department of Chemistry, Northwestern University, Evanston, Illinois 60208, United States;* orcid.org/0000-0001-5852-9757

Yuanning Feng – *Department of Chemistry, Northwestern University, Evanston, Illinois 60208, United States;* orcid.org/0000-0002-8832-0767

Fangjun Liu – *Department of Chemistry, Stoddart Institute of Molecular Science, Zhejiang University, Hangzhou 310027, China; ZJU-Hangzhou Global Scientific and Technological Innovation Center, Hangzhou 311215, China*

Complete contact information is available at: https://pubs.acs.org/10.1021/jacs.2c13846

Notes

The authors declare no competing financial interest.

■ ACKNOWLEDGMENTS

We thank Northwestern University (NU) for continued support of this research. This work made use of the IMSERC NMR facility at NU, which receives support from the Soft and Hybrid Nanotechnology Experimental (SHyNE) Resource (NSF ECCS-2025633) and NU. Transient absorption spectroscopy was supported by the National Science Foundation (DMR-2003739) (M.S.M., R.M.Y., and M.R.W.). Research at Zhejiang University was supported by the Starry Night Science Fund of the Zhejiang University Shanghai Institute for Advanced Study (no. SN-ZJU-SIAS-006) and the National Natural Science Foundation of China (22273085). The authors thank Professor Haiyan Qin, Chuyue Li, and Jing Wang from Department of Chemistry at Zhejiang University for the assistance in quantum yield measurement. The authors also thank Shanghai ShengSheng Logistics for the financial support.

■ REFERENCES

(1) Zhou, J.; Liu, Q.; Feng, W.; Sun, Y.; Li, F. Upconversion luminescent materials: Advances and applications. *Chem. Rev.* **2015**, *115*, 395−465.

(2) Zhou, W.; Shang, Y.; García de Arquer, F. P.; Xu, K.; Wang, R.; Luo, S.; Xiao, X.; Zhou, X.; Huang, R.; Sargent, E. H.; Ning, Z. Solution-processed upconversion photodetectors based on quantum dots. *Nat. Electron.* **2020**, *3*, 251−258.

(3) De Wild, J.; Meijerink, A.; Rath, J. K.; van Sark, W. G. J. H. M.; Schropp, R. E. I. Upconverter solar cells: Materials and applications. *Energy Environ. Sci.* **2011**, *4*, 4835−4848.

(4) Richards, B. S.; Hudry, D.; Busko, D.; Turshatov, A.; Howard, I. A. Photon upconversion for photovoltaics and photocatalysis: A critical review. *Chem. Rev.* **2021**, *121*, 9165−9195.

(5) Huang, X.; Han, S.; Huang, W.; Liu, X. Enhancing solar cell efficiency: The search for luminescent materials as spectral converters. *Chem. Soc. Rev.* **2013**, *42*, 173−201.

(6) Jones, A. M.; Yu, H.; Schaibley, J. R.; Yan, J.; Mandrus, D. G.; Taniguchi, T.; Watanabe, K.; Dery, H.; Yao, W.; Xu, X. Excitonic luminescence upconversion in a two-dimensional semiconductor. *Nat. Phys.* **2016**, *12*, 323−327.

(7) Fernandez-Bravo, A.; Yao, K.; Barnard, E. S.; Borys, N. J.; Levy, E. S.; Tian, B.; Tajon, C. A.; Moretti, L.; Altoe, M. V.; Aloni, S.; Beketayev, K.; Scotognella, F.; Cohen, B. E.; Chan, E. M.; Schuck, P. J. Continuous-wave upconverting nanoparticle microlasers. *Nat. Nanotechnol.* **2018**, *13*, 572−577.

(8) Mattiello, S.; Mecca, S.; Ronchi, A.; Calascibetta, A.; Mattioli, G.; Pallini, F.; Meinardi, F.; Beverina, L.; Monguzzi, A. Diffusion-free intramolecular triplet−triplet annihilation in engineered conjugated chromophores for sensitized photon upconversion. *ACS Energy Lett.* **2022**, *7*, 2435−2442.

(9) Perego, J.; Pedrini, J.; Bezuidenhout, C. X.; Sozzani, P. E.; Meinardi, F.; Bracco, S.; Comotti, A.; Monguzzi, A. Engineering porous emitting framework nanoparticles with integrated sensitizers for low-power photon upconversion by triplet fusion. *Adv. Mater.* **2019**, *31*, No. e1903309.

(10) Wang, F.; Banerjee, D.; Liu, Y.; Chen, X.; Liu, X. Upconversion nanoparticles in biological labeling, imaging, and therapy. *Analyst* **2010**, *135*, 1839−1854.

(11) Chen, G.; Qiu, H.; Prasad, P. N.; Chen, X. Upconversion nanoparticles: design, nanochemistry, and applications in theranostics. *Chem. Rev.* **2014**, *114*, 5161−5214.

(12) Askes, S. H. C.; Bonnet, S. Solving the oxygen sensitivity of sensitized photon upconversion in life science applications. *Nat. Rev. Chem.* **2018**, *2*, 437−452.

(13) Park, J.; Xu, M.; Li, F.; Zhou, H.-C. 3D Long-range triplet migration in a water-stable metal−organic framework for upconversion-based ultralow-power in vivo imaging. *J. Am. Chem. Soc.* **2018**, *140*, 5493−5499.

(14) Parker, C. A.; Hatchard, C. G.; Bowen, E. J. Delayed fluorescence from solutions of anthracene and phenanthrene. *Proc. R. Soc. A* **1962**, *269*, 574−584.

(15) Parker, C. A.; Bowen, E. J. Sensitized P-type delayed fluorescence. *Proc. R. Soc. A* **1963**, *276*, 125−135.

(16) Ronchi, A.; Monguzzi, A. Sensitized triplet−triplet annihilation based photon upconversion in full organic and hybrid multicomponent systems. *Chem. Phys. Rev.* **2022**, *3*, No. 041301.

(17) Wu, W.; Zhao, J.; Sun, J.; Guo, S. Light-harvesting fullerene dyads as organic triplet photosensitizers for triplet−triplet annihilation upconversions. *J. Org. Chem.* **2012**, *77*, 5305−5312.

(18) Zhao, J.; Wu, W.; Sun, J.; Guo, S. Triplet photosensitizers: From molecular design to applications. *Chem. Soc. Rev.* **2013**, *42*, 5323−5351.

(19) Gray, V.; Dzebo, D.; Abrahamsson, M.; Albinsson, B.; Moth-Poulsen, K. Triplet−triplet annihilation photon-upconversion: Towards solar energy applications. *Phys. Chem. Chem. Phys.* **2014**, *16*, 10345−10352.

(20) Huang, L.; Le, T.; Huang, K.; Han, G. Enzymatic enhancing of triplet−triplet annihilation upconversion by breaking oxygen quench-

ing for background-free biological sensing. *Nat. Commun.* **2021**, *12*, 1898.
(21) Hiroto, S.; Miyake, Y.; Shinokubo, H. Synthesis and functionalization of porphyrins through organometallic methodologies. *Chem. Rev.* **2017**, *117*, 2910−3043.
(22) Sessler, J. L.; Gross, Z.; Furuta, H. Expanded, contracted, and isomeric porphyrins. *Chem. Rev.* **2017**, *117*, 2201−2202.
(23) Kim, J.-H.; Deng, F.; Castellano, F. N.; Kim, J.-H. Red-to-blue/cyan/green upconverting microcapsules for aqueous- and dry-phase color tuning and magnetic sorting. *ACS Photonics* **2014**, *1*, 382−388.
(24) Hoseinkhani, S.; Tubino, R.; Meinardi, F.; Monguzzi, A. Achieving the photon up-conversion thermodynamic yield upper limit by sensitized triplet−triplet annihilation. *Phys. Chem. Chem. Phys.* **2015**, *17*, 4020−4024.
(25) Li, C.; Koenigsmann, C.; Deng, F.; Hagstrom, A.; Schmuttenmaer, C. A.; Kim, J.-H. Photocurrent enhancement from solid-state triplet−triplet annihilation upconversion of low-intensity, low-energy photons. *ACS Photonics* **2016**, *3*, 784−790.
(26) Ravetz, B. D.; Pun, A. B.; Churchill, E. M.; Congreve, D. N.; Rovis, T.; Campos, L. M. Photoredox catalysis using infrared light via triplet fusion upconversion. *Nature* **2019**, *565*, 343−346.
(27) Nonat, A.; Bahamyirou, S.; Lecointre, A.; Przybilla, F.; Mély, Y.; Platas-Iglesias, C.; Camerel, F.; Jeannin, O.; Charbonnière, L. J. Molecular upconversion in water in heteropolynuclear supramolecular Tb/Yb assemblies. *J. Am. Chem. Soc.* **2019**, *141*, 1568−1576.
(28) Xu, W.; Liang, W.; Wu, W.; Fan, C.; Rao, M.; Su, D.; Zhong, Z.; Yang, C. Supramolecular assembly-improved triplet−triplet annihilation upconversion in aqueous solution. *Chem. − Eur. J.* **2018**, *24*, 16677−16685.
(29) Lai, H.; Zhao, T.; Deng, Y.; Fan, C.; Wu, W.; Yang, C. Assembly-enhanced triplet-triplet annihilation upconversion in the aggregation formed by Schiff-base Pt(II) complex grafting-permethyl-β-CD and 9, 10-diphenylanthracence dimer. *Chin. Chem. Lett.* **2019**, *30*, 1979−1983.
(30) Wu, W.; Ji, S.; Wu, W.; Shao, J.; Guo, H.; James, T. D.; Zhao, J. Ruthenium(II)−polyimine−coumarin light-harvesting molecular arrays: Design rationale and application for triplet−triplet-annihilation-based upconversion. *Chem. − Eur. J.* **2012**, *18*, 4953−4964.
(31) Ballester, P.; Fujita, M.; Rebek, J. Molecular containers. *Chem. Soc. Rev.* **2015**, *44*, 392−393.
(32) Zarra, S.; Wood, D. M.; Roberts, D. A.; Nitschke, J. R. Molecular containers in complex chemical systems. *Chem. Soc. Rev.* **2015**, *44*, 419−432.
(33) Liu, W.; Stoddart, J. F. Emergent behavior in nanoconfined molecular containers. *Chem* **2021**, *7*, 919−947.
(34) Roy, I.; Bobbala, S.; Young, R. M.; Beldjoudi, Y.; Nguyen, M. T.; Cetin, M. M.; Cooper, J. A.; Allen, S.; Anamimoghadam, O.; Scott, E. A.; Wasielewski, M. R.; Stoddart, J. F. A supramolecular approach for modulated photoprotection, lysosomal delivery, and photodynamic activity of a photosensitizer. *J. Am. Chem. Soc.* **2019**, *141*, 12296−12304.
(35) Roy, I.; Garci, A.; Beldjoudi, Y.; Young, R. M.; Pe, D. J.; Nguyen, M. T.; Das, P. J.; Wasielewski, M. R.; Stoddart, J. F. Host−guest complexation-mediated supramolecular photon upconversion. *J. Am. Chem. Soc.* **2020**, *142*, 16600−16609.
(36) Joarder, B.; Yanai, N.; Kimizuka, N. Solid-state photon upconversion materials: Structural integrity and triplet−singlet dual energy migration. *J. Phys. Chem. Lett.* **2018**, *9*, 4613−4624.
(37) Cram, D. J.; Cram, J. M. Host-guest chemistry. *Science* **1974**, *183*, 803−809.
(38) Fan, C.; Wu, W.; Chruma, J. J.; Zhao, J.; Yang, C. Enhanced triplet−triplet energy transfer and upconversion fluorescence through host−guest complexation. *J. Am. Chem. Soc.* **2016**, *138*, 15405−15412.
(39) Simon, Y. C.; Weder, C. Low-power photon upconversion through triplet−triplet annihilation in polymers. *J. Mater. Chem.* **2012**, *22*, 20817−20830.
(40) Benson, C. R.; Kacenauskaite, L.; VanDenburgh, K. L.; Zhao, W.; Qiao, B.; Sadhukhan, T.; Pink, M.; Chen, J.; Borgi, S.; Chen, C.-H.; Davis, B. J.; Simon, Y. C.; Raghavachari, K.; Laursen, B. W.; Flood, A. H. Plug-and-play optical materials from fluorescent dyes and macrocycles. *Chem* **2020**, *6*, 1978−1997.
(41) Gray, V.; Moth-Poulsen, K.; Albinsson, B.; Abrahamsson, M. Towards efficient solid-state triplet−triplet annihilation based photon upconversion: Supramolecular, macromolecular and self-assembled systems. *Coord. Chem. Rev.* **2018**, *362*, 54−71.
(42) Shi, Y.; Cai, K.; Xiao, H.; Liu, Z.; Zhou, J.; Shen, D.; Qiu, Y.; Guo, Q.-H.; Stern, C.; Wasielewski, M. R.; Diederich, F.; Goddard, W. A., III; Stoddart, J. F. Selective extraction of C_{70} by a tetragonal prismatic porphyrin cage. *J. Am. Chem. Soc.* **2018**, *140*, 13835−13842.
(43) Durot, S.; Taesch, J.; Heitz, V. Multiporphyrinic cages: Architectures and functions. *Chem. Rev.* **2014**, *114*, 8542−8578.
(44) Elemans, J. A. A. W.; Nolte, R. J. M. Porphyrin cage compounds based on glycoluril − From enzyme mimics to functional molecular machines. *Chem. Commun.* **2019**, *55*, 9590−9605.
(45) Zhu, H.; Li, Q.; Shi, B.; Ge, F.; Liu, Y.; Mao, Z.; Zhu, H.; Wang, S.; Yu, G.; Huang, F.; Stang, P. J. Dual-emissive platinum(II) metallacage with a sensitive oxygen response for imaging of hypoxia and imaging-guided chemotherapy. *Angew. Chem., Int. Ed.* **2020**, *59*, 20208−20214.
(46) Yu, G.; Yu, S.; Saha, M. L.; Zhou, J.; Cook, T. R.; Yung, B. C.; Chen, J.; Mao, Z.; Zhang, F.; Zhou, Z.; Liu, Y.; Shao, L.; Wang, S.; Gao, C.; Huang, F.; Stang, P. J.; Chen, X. A discrete organoplatinum(II) metallacage as a multimodality theranostic platform for cancer photochemotherapy. *Nat. Commun.* **2018**, *9*, 4335.
(47) Hong, S.; Rohman, M. R.; Jia, J.; Kim, Y.; Moon, D.; Kim, Y.; Ko, Y. H.; Lee, E.; Kim, K. Porphyrin boxes: Rationally designed porous organic cages. *Angew. Chem., Int. Ed.* **2015**, *54*, 13241−13244.
(48) Smith, P. T.; Benke, B. P.; Cao, Z.; Kim, Y.; Nichols, E. M.; Kim, K.; Chang, C. J. Iron porphyrins embedded into a supramolecular porous organic cage for electrochemical CO_2 reduction in water. *Angew. Chem., Int. Ed.* **2018**, *57*, 9684−9688.
(49) Kim, Y.; Koo, J.; Hwang, I.-C.; Mukhopadhyay, R. D.; Hong, S.; Yoo, J.; Dar, A. A.; Kim, I.; Moon, D.; Shin, T. J.; Ko, Y. H.; Kim, K. Rational design and construction of hierarchical superstructures using shape-persistent organic cages: Porphyrin box-based metallosupramolecular assemblies. *J. Am. Chem. Soc.* **2018**, *140*, 14547−14551.
(50) Koo, J.; Kim, I.; Kim, Y.; Cho, D.; Hwang, I.-C.; Mukhopadhyay, R. D.; Song, H.; Ko, Y. H.; Dhamija, A.; Lee, H.; Hwang, W.; Kim, S.; Baik, M.-H.; Kim, K. Gigantic porphyrinic cages. *Chem* **2020**, *6*, 3374−3384.
(51) Chen, T.; Li, M.; Liu, J. $\pi-\pi$ Stacking interaction: A nondestructive and facile means in material engineering for bioapplications. *Cryst. Growth Des.* **2018**, *18*, 2765−2783.
(52) Zhang, J.; Li, Y.; Yang, W.; Lai, S.-W.; Zhou, C.; Liu, H.; Che, C.-M.; Li, Y. A smart porphyrin cage for recognizing azide anions. *Chem. Commun.* **2012**, *48*, 3602−3604.
(53) Zhang, Z.; Ma, L.; Fang, F.; Hou, Y.; Lu, C.; Mu, C.; Zhang, Y.; Liu, H.; Gao, K.; Wang, M.; Zhang, Z.; Li, X.; Zhang, M. Porphyrin-based multicomponent metallacage: Host−guest complexation toward photooxidation-triggered reversible encapsulation and release. *JACS Au* **2022**, *2*, 1479−1487.
(54) Yu, G.; Ye, Y.; Tong, Z.; Yang, J.; Li, Z.; Hua, B.; Shao, L.; Li, S. A porphyrin-based discrete tetragonal prismatic cage: Host−guest complexation and its application in tuning liquid-crystalline behavior. *Macromol. Rapid Commun.* **2016**, *37*, 1540−1547.
(55) Rothschild, D. A.; Kopcha, W. P.; Tran, A.; Zhang, J.; Lipke, M. C. Gram-scale synthesis of a covalent nanocage that preserves the redox properties of encapsulated fullerenes. *Chem. Sci.* **2022**, *13*, 5325−5332.
(56) Brenner, W.; Ronson, T. K.; Nitschke, J. R. Separation and selective formation of fullerene adducts within an $M^{II}_8L_6$ cage. *J. Am. Chem. Soc.* **2017**, *139*, 75−78.
(57) García-Simón, C.; Monferrer, A.; Garcia-Borràs, M.; Imaz, I.; Maspoch, D.; Costas, M.; Ribas, X. Size-selective encapsulation of C_{60} and C_{60}-derivatives within an adaptable naphthalene-based tetragonal prismatic supramolecular nanocapsule. *Chem. Commun.* **2019**, *55*, 798−801.

https://doi.org/10.1021/jacs.2c13846
J. Am. Chem. Soc. 2023, 145, 10061−10070

(58) Rizzuto, F. J.; Wood, D. M.; Ronson, T. K.; Nitschke, J. R. Tuning the redox properties of fullerene clusters within a metal−organic capsule. *J. Am. Chem. Soc.* **2017**, *139*, 11008−11011.
(59) Nobukuni, H.; Shimazaki, Y.; Uno, H.; Naruta, Y.; Ohkubo, K.; Kojima, T.; Fukuzumi, S.; Seki, S.; Sakai, H.; Hasobe, T.; Tani, F. Supramolecular structures and photoelectronic properties of the inclusion complex of a cyclic free-base porphyrin dimer and C_{60}. *Chem. − Eur. J.* **2010**, *16*, 11611−11623.
(60) Song, J.; Aratani, N.; Shinokubo, H.; Osuka, A. A porphyrin nanobarrel that encapsulates C_{60}. *J. Am. Chem. Soc.* **2010**, *132*, 16356−16357.
(61) Zhang, C.; Wang, Q.; Long, H.; Zhang, W. A highly C_{70} selective shape-persistent rectangular prism constructed through one-step alkyne metathesis. *J. Am. Chem. Soc.* **2011**, *133*, 20995−21001.
(62) Hajjaj, F.; Tashiro, K.; Nikawa, H.; Mizorogi, N.; Akasaka, T.; Nagase, S.; Furukawa, K.; Kato, T.; Aida, T. Ferromagnetic spin coupling between endohedral metallofullerene La@C_{82} and a cyclodimeric copper porphyrin upon inclusion. *J. Am. Chem. Soc.* **2011**, *133*, 9290−9292.
(63) Schmittel, M.; He, B.; Mal, P. Supramolecular multicomponent self-assembly of shape-adaptive nanoprisms: Wrapping up C_{60} with three porphyrin units. *Org. Lett.* **2008**, *10*, 2513−2516.
(64) Nakamura, T.; Ube, H.; Miyake, R.; Shionoya, M. A C_{60}-templated tetrameric porphyrin barrel complex via zinc-mediated self-assembly utilizing labile capping ligands. *J. Am. Chem. Soc.* **2013**, *135*, 18790−18793.
(65) Kieran, A. L.; Pascu, S. I.; Jarrosson, T.; Sanders, J. K. M. Inclusion of C_{60} into an adjustable porphyrin dimer generated by dynamic disulfide chemistry. *Chem. Commun.* **2005**, 1276−1278.
(66) Mukhopadhyay, R. D.; Kim, Y.; Koo, J.; Kim, K. Porphyrin boxes. *Acc. Chem. Res.* **2018**, *51*, 2730−2738.
(67) Yu, X.; Wang, B.; Kim, Y.; Park, J.; Ghosh, S.; Dhara, B.; Mukhopadhyay, R. D.; Koo, J.; Kim, I.; Kim, S.; Hwang, I.-C.; Seki, S.; Guldi, D. M.; Baik, M.-H.; Kim, K. Supramolecular fullerene tetramers concocted with porphyrin boxes enable efficient charge separation and delocalization. *J. Am. Chem. Soc.* **2020**, *142*, 12596−12601.
(68) Dhamija, A.; Das, C. K.; Ko, Y. H.; Kim, Y.; Mukhopadhyay, R. D.; Gunnam, A.; Yu, X.; Hwang, I.-C.; Schäfer, L. V.; Kim, K. Remotely controllable supramolecular rotor mounted inside a porphyrinic cage. *Chem* **2022**, *8*, 543−556.
(69) Cook, R. E.; Phelan, B. T.; Kamire, R. J.; Majewski, M. B.; Young, R. M.; Wasielewski, M. R. Excimer formation and symmetry-breaking charge transfer in cofacial perylene dimers. *J. Phys. Chem. A* **2017**, *121*, 1607−1615.
(70) Nagai, A.; Miller, J. B.; Kos, P.; Elkassih, S.; Xiong, H.; Siegwart, D. J. Tumor imaging based on photon upconversion of Pt(II) porphyrin rhodamine co-modified NIR excitable cellulose enhanced by aggregation. *ACS Biomater. Sci. Eng.* **2015**, *1*, 1206−1210.
(71) Gouterman, M.; Khalil, G.-E. Porphyrin free base phosphorescence. *J. Mol. Spectrosc.* **1974**, *53*, 88−100.
(72) Clarke, R. H.; Hochstrasser, R. M. Location and assignment of the lowest triplet state of perylene. *J. Mol. Spectrosc.* **1969**, *32*, 309−319.
(73) Fathalla, M.; Barnes, J. C.; Young, R. M.; Hartlieb, K. J.; Dyar, S. M.; Eaton, S. W.; Sarjeant, A. A.; Co, D. T.; Wasielewski, M. R.; Stoddart, J. F. Photoinduced electron transfer within a zinc porphyrin−cyclobis(paraquat-*p*-phenylene) donor−acceptor dyad. *Chem. − Eur. J.* **2014**, *20*, 14690−14697.
(74) Alqahtani, N. Z.; Blevins, T. G.; McCusker, C. E. Quantifying triplet state formation in zinc dipyrrin complexes. *J. Phys. Chem. A* **2019**, *123*, 10011−10018.
(75) Young, R. M.; Jensen, S. C.; Edme, K.; Wu, Y.; Krzyaniak, M. D.; Vermeulen, N. A.; Dale, E. J.; Stoddart, J. F.; Weiss, E. A.; Wasielewski, M. R.; Co, D. T. Ultrafast two-electron transfer in a CdS quantum dot−extended-viologen cyclophane complex. *J. Am. Chem. Soc.* **2016**, *138*, 6163−6170.
(76) Monguzzi, A.; Mauri, M.; Frigoli, M.; Pedrini, J.; Simonutti, R.; Larpent, C.; Vaccaro, G.; Sassi, M.; Meinardi, F. Unraveling triplet excitons photophysics in hyper-cross-linked polymeric nanoparticles: Toward the next generation of solid-state upconverting materials. *J. Phys. Chem. Lett.* **2016**, *7*, 2779−2785.
(77) Narioka, S.; Ishii, H.; Ouchi, Y.; Yokoyama, T.; Ohta, T.; Seki, K. XANES Spectroscopic studies of evaporated porphyrin films: molecular orientation and electronic structure. *J. Phys. Chem.* **1995**, *99*, 1332−1337.

https://doi.org/10.1021/jacs.2c13846
J. Am. Chem. Soc. 2023, 145, 10061−10070